INTERNATIONAL JOURNAL OF SCIENCE AND NATURE

www.scienceandnature.org

ROLE OF SULFUR CONTENT ON THE PHOTO DETECTION PARAMETERS OF AgSb $(S_xSe_{1-x})_2$ THIN FILMS

Bushra A. Hasan
University of Baghdad, College of Science, Department of Physics

ABSTRACT
Silver antimony sulfoselenide alloys with various sulfur content were obtained using quenching the melt method. The obtained alloys $AgSb(S_xSe_{1-x})_2$ were used to prepare thin films with different sulfur concentration at room temperature 303K on glass substrate using pulsed laser deposition under vacuum of 10^{-2} bar, thickness of ~100nm. The structure of the prepared alloys and thin films were checked using x-ray diffraction. Measurements of X-ray showed that the prepared alloys have polycrystalline with cubic structure while the prepared thin films were amorphous. Atomic Force Microscopy revealed that the average particle size decreases while roughness showed non systematic increase with the increase of sulphur concentration. Optical properties measurements showed that the prepared thin films have indirect allowed band gap which tend to increase with the increase of sulphur concentration, the optical energy gap increases from 1.1 to 1.7 eV with the increase of sulphur concentration .The dark conductivity and photoconductivity of $AgSb(S_{0.2}Se_{0.8})_2$/n, p-Siand $(AgSb(S_{0.4}Se_{0.6})_2$/n, p-Si were measured. The results indicate that increase of sulphur concentration in the thin films of quaternary system worsen $\Delta\sigma/\sigma$.

KEYWORDS: AgSb $(S_xSe_{1-x})_2$ thin films, photoconductivity, optical band gap.

INTRODUCTION

Recently solar cell material research have considered "earth-abundant" light absorber materials as alternatives to Cu (In,Ga)Se_2 and CdTe to avoid high toxicity of cadmium and insufficiency of indium[1]. Alloys based on $AgSbSe_2$ are considered as promising materials for solar cell applications, as a result of high optical absorption coefficient of 10^4 cm^{-1} and band gap of 0.9-1.1 eV[2,3]. Promising results provided from $AgSbSe_2$ as absorber which prepared by and Photovoltaic structures using absorber thin films prepared by heating multilayer's of Sb_2S_3/Ag_2 Se and CdS window layer[4]. Efficiency of more than 2% from this photovoltaic structure was obtained[5]. Another method which is Pulsed laser deposition (PLD) provided better control over the process parameters on the thin films as well as it is a fast method[6]. On the other hand best control of material morphologies with lowest loss of precursors[7], Fast controlling on selenization[8,9] and PV parameters were enhanced throughout Na incorporation in CIGS [10-12]. Many researches concerned on chalcogenides phases due an Unique ferroelectric, thermoelectric and non-linear optical properties .Such as the compounds $AASe_2$ where (A = Li, Na) and $AgSbQ_2$ (Q=S, Se)[13-18]. An additional modification of the $AgSbS_2$ ternary phase is the compounds like $(MS)_{1-x}$ $(AgSbS_2)_x$ which are semiconductors with narrow optical gaps in the range from 0.01 to 0.6 eV[19]. The electrical measurement of these materials indicated that these phases present ionic or mixed (electronic-ionic) transport via silver cations. β-$AgSbS_2$ found in cubic phase at high temperature. It switches to the monoclinic α-$AgSbS_2$ phase, at low temperature[20]. The crystalline structure of the α -$AgSbS_2$ was investigated by many authors: Hofmann (1938); Knowles (1964) and Smith *et al*. (1997); however, Effenberger *et al.* (2002) have shown that the chains of connected SbS_3 pyramids [21]. While the chains are linked by linear S-Ag-S and AgS_4 polyhedra. The electrical conductivity was 10^{-6} S/m in single crystals with band-gaps in the range of 1.23-1.73 eV [22]. On the other hand amorphous chalcogenides films of Ge, As, Sb, Te, Ag, In and other elements, with binary or multinary elements compositions) have got many applications like in micro optics, photonic crystals and optical memories[23-24]. Wagner *et al*. [2004][25] prepared amorphous films of $Sb_{33}S_{67}$ and $Ag_x(Sb_{0.33}S_{0.67})_{100-x}$with different composition, where x is between 0 and 25 at.% Ag, using different methods like thermal evaporation under vacuum, optically-induced silver dissolution into the binary Sb-S chalcogenides deposited by vacuum evaporation and spin coating. Thin films of $AgSbSe_2$ were prepared by Bindu *et al*. [2005][26] using two stages of processes. They obtained band gap of 0.9 eV. Measurement of thermoelectric indicated a See beck coefficient of 500 $\mu V\ K^{-1}$ (p-type), and a hole concentration of ~10^{22} m^{-3}. They also illustrated the feasibility of application of these films as a photovoltaic absorber material for the structure SnO_2–CdS–(i) Sb_2S_3–(p) $AgSbSe_2$, open circuit voltage of 530 mV was obtained under an intensity of illumination of 2 kW m^{-2}. Tasseva *et al*. [2007][27]presented results of investigations of optically uniform thin $As_{33}S_{67-x}Se_x$ ($0\le x\le 67$) films deposited by thermal evaporation on glass substrates. Bulk alloys samples were synthesized by melting pure elements As, S and Se in a quartz ampoule at 760°C for 12 hours. The changes in optical properties like transmittance, reflectance, refractive index and optical band gap in the visible and NIR region of thin films (700 nm thick) depending on composition and exposure to light have been studied. The photo-induced diffusion of Ag into As-S-Se thin films was studied using glass substrates with initially deposited by RF sputtering Ag films with

different thickness. In the previous work I have reported the preparation of $AgSb(S_xSe_{1-x})_2$ thin films with sulfur concentration x=0 by thermal evaporation technique as photodetector[28]. The present study reports the synthesizing of the quaternary alloys $AgSb(S_xSe_{1-x})_2$ with various composition ratios(x=0.2,0.4,0.8, and 1.0) and then obtains thin films samples from theses alloys using pulsed laser deposition. The influence of composition ratio on the structure, morphology and conductivity in dark and under illumination were studied. Characterization of the $AgSb(S_xSe_{1-x)2}$ materials was performed using X-ray diffraction, Atomic Force Microscopy. The structure, morphology, composition, optical energy gap and electrical conductivity of the films were analyzed using X-ray diffractometer (XRD), Atomic Force Microscope (AFM), energy dispersive spectroscopy EDS, and UV-Vis-NIR spectrophotometer. Our object is to synthesize silver antimony sulfoselenide $AgSb(S_xSe_{1-x})_2$ alloys with different composition (0.2,0.4,0.8 and 1.0), No one has ever tried to synthesis them by quenching from the melt. Persuaded by the previous results have been used pulsed laser deposition PLD process to develop $AgSb(S_xSe_{1-x})_2$ photodetector thin films.

Experimental Part

Alloys of $AgSb(S_xSe_{1-x})_2$ were obtained by quenching technique. The exact amount of high purity (99.999%) obtained from Certified Chemicals, UK and (99.95%) antimony obtained from Fluca, Germany, (Ag, Sb, S and Se) elements accordance with their atomic percentages ($AgSb(S_{0.2}Se_{0.8})_2$, $AgSb(S_{0.4}Se_{0.6})_2$ $AgSb(S_{0.8}Se_{0.2})_2$ and $AgSbS_2$ are weighed using an electronic balance with the least count of (10^{-4} g). The material was then sealed in evacuated (~10^{-5} Torr) quartz ampoule (length ~ 25 cm and internal diameter ~ 8 mm). The ampoules containing material are heated to 1000 ^oC for all compositions ratio for 5 hours. The temperature of the furnace was raised at a rate of 10 ^oC/min. During heating the ampoules are constantly rocked to obtain homogeneous alloys. After that the obtained melt left to cool in air. Thin films from $AgSb(S_xSe_{1-x})_2$ with different compositions were prepared by PLD technique. The pulsed laser deposition experiment was carried out inside a vacuum chamber generally at (10^{-3} Torr) vacuum conditions. The focused Nd: YAG Q-switching laser beam was coming through a window to incident on the target surface at an angle 45°. The substrate was placed in front of the target with its surface parallel to the target. Sufficient gap was kept between the target and the substrate so that the substrate holder did not obstruct the incident laser beam. Nd: YAG laser (Huafei Tongda Technology—DIAMOND-288 pattern EPLS) was used for the deposition of $AgSb(S_xSe_{1-x})_2$ on different substrates. The main technical parameters are :Laser model: Q-switched Nd: YAG Laser Second Harmonic Generation (SHG), Laser wavelength: (1064 /532) nm, Energy density (0.8- 1.8) J/cm^2,10 ns pulse duration, Repetition frequency: (6) Hz, Cooling method: inner circulation water cooling Power supply: 220V.In this work, corning glass substrates, single crystals of (111) orientation n-Si, (001) orientation p-Si and (111) orientation are employed. The procedures for cleaning the glass substrates are as follows:

1. They are cleaned using detergent with water to remove any oil or dust that might be attached to the surface of substrate and then placed under tap water and rubbing gently for 15 minutes.
2. They are then placed in a clean beaker containing distilled water and then rinsed in ultrasonic unit for 15 minutes.
3. Step 2 is repeated by replacing the distilled water with pure alcohol solution which reacts with contamination such as grease and some oxides.
4. The slides eventually are dried by blowing air and wiped with soft tissue.

While single crystal silicon wavers were etched in solution of 1vol of HF+9 vol of distil water. The thickness of the prepared thin films were estimated using Fizeau fringes technique of equal thickness ,the film thickness(t) is given by:

$$t = \frac{\lambda}{2}.\frac{\Delta x}{x} \quad \text{.....(1)}$$

Where Δx is the shift between the interference fringes, X is the distance between the interference fringes and λ is the He: Ne wavelength (6320 Å). The chemical composition of the prepared alloys was checked using energy dispersive X-ray unit interfaced with a scanning electron microscope (Type JEOL-JSGM-T200). The microstructure of the prepared thin films was also examined using atomic force microscopy (Type JEOL-JSGM-T1230). A double beam spectrophotometer, with automatic computer data acquisition (Type Jasco, V-570, Rerll-00, and UV–VIS) absorbance and transmittance, was employed at normal light incidence to record the optical transmission and reflection spectra of the deposited thin films over the wavelength range 200–1100 nm. The dark current of $AgSb(S_xSe_{1-x})_2$ photoconductive films at sulfur content was measured as a function of applied voltage (0-6 Volt). The current-voltage measurement in the dark of $AgSb(S_xSe_{1-x})_2$ photodetectors with different value of x content and thickness are done by using Keithly Digital Electrometer 616 and D.C power supply. The dark and the photo current of photodetectors at bias voltage (0-5) V in the case of forward connections measured. I-V measurements have been done in dark and under illumination with Halogen lamp type Philips 120W at intensity 100mW/cm^2 by using. s the distance between the electrode and A is the sample area .

RESULTS & DISCUSSION

The elemental compositions analysis of the $AgSb(S_xSe_{1-x})_2$ alloys with various sulfur concentration were checked throughout Energy Dispersive spectroscopy (EDS). The results display in figure 1 and Table. 1

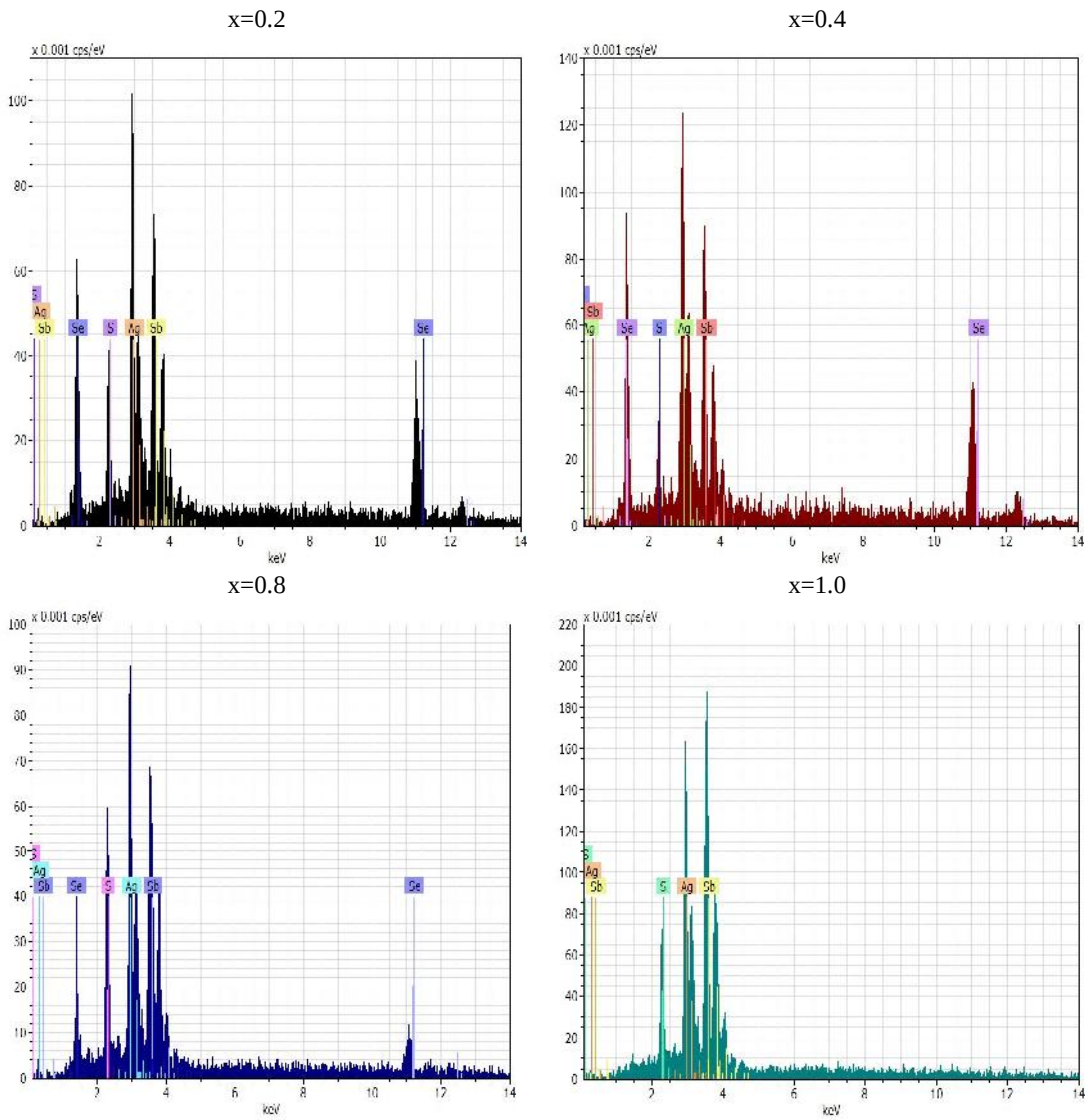

FIGURE 1: EDAX images of $AgSb(S_xSe_{1-x})_2$ alloys with various sulfur content

TABLE 1. Composition analysis DATAof $AgSb(S_xSe_{1-x})_2$alloys using (EDX) technique.

Alloy	Theoretical concentration				Experimental concentration			
	Ag	Sb	S	Se	Ag	Sb	S	Se
$AgSb(S_{0.2}Se_{0.8})_2$	33.34	33.34	6.68	26.72	34.58	33.68	5.68	26.05
$AgSb(S_{0.4}Se_{0.6})_2$	33.34	33.34	13.36	20.04	38.13	36.48	11.86	18.93
$AgSb(S_{0.8}Se_{0.2})_2$	33.34	33.34	26.72	6.68	33.25	33.33	28.03	5.38
$AgSbS_2$	33.34	33.34	33.34	0	33.17	33.17	33.64	0

The x-ray diffraction pattern of $AgSb(S_xSe_{1-x})_2$ alloys prepared from quenching the melt with various composition is shown in Fig.2. From the figure, it is obvious the dominant peaks of cubic $AgSb(S_xSe_{1-x})_2$ phase as pointed out by previous studies [29] indexed by (111), (200) and (220) planes were appeared. This confirms the formation of quaternary system. All other diffraction peaks present in the alloy identified as Ag_5SbS_4 phase (PDF 96-900-7511) as marked in the figure. As the composition ratio increased, these quaternary dominant peaks intensities were decreased as seen in Fig. 1(a-d), while the grain size increased in the first and then decreases with further increase of sulfur content. It is obvious there are no other phases of Ag-Sb-S-Se compositions such as monoclinic phase.

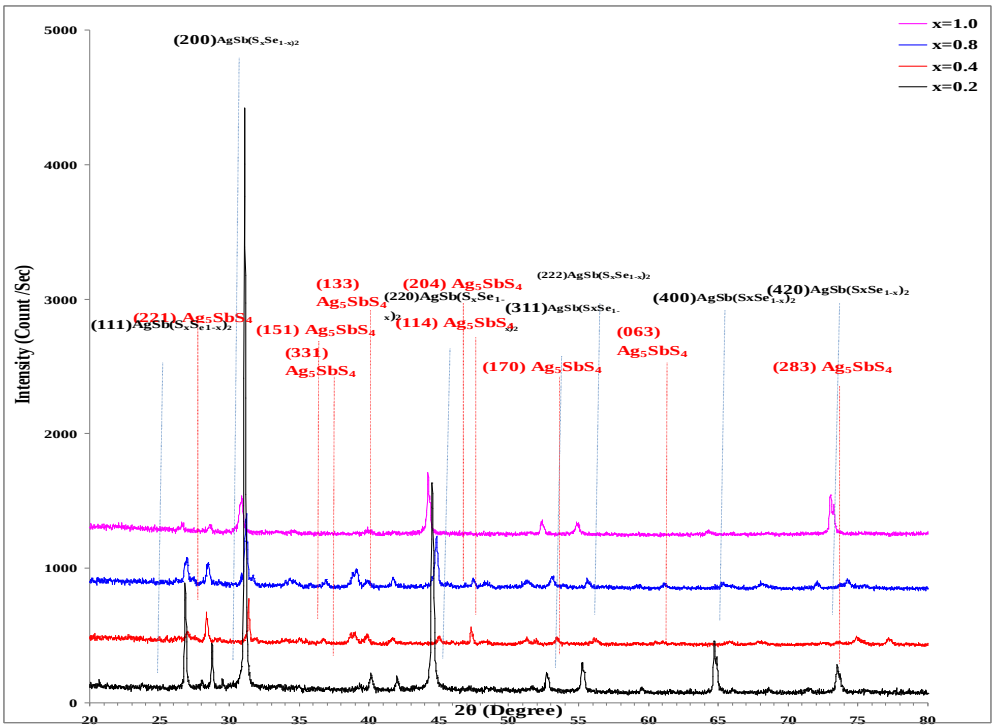

FIGURE 2: XRD of $AgSb(S_xSe_{1-x})_2$ alloys with different compositions.

TABLE 2: X-ray diffraction data of $AgSb(S_xSe_{1-x})_2$ alloys with sulfur content

Sample	2θ (Deg.)	FWHM (Deg.)	d_{hkl} Exp.(Å)	G.S (nm)	d_{hkl} Std.(Å)	Phase	hkl	card No.
	26.8719	0.2217	3.3151	36.8	3.3405	$AgSb(S_xSe_{1-x})_2$	(111)	Ref.[29]
	28.7931	0.1478	3.0982	55.5	3.1032	Ag_5SbS_4	(221)	96-900-7511
	31.1576	0.2955	2.8682	27.9	2.8930	$AgSb(S_xSe_{1-x})_2$	(200)	Ref.[29]
	39.2857	0.5173	2.2915	16.3	2.2908	Ag_5SbS_4	(151)	96-900-7511
	40.1724	0.3695	2.2429	22.9	2.2576	Ag_5SbS_4	(133)	96-900-7511
x=0.2	42.0197	0.2217	2.1485	38.4	2.1483	Ag_5SbS_4	(331)	96-900-7511
	44.5320	0.2217	2.0330	38.7	2.0457	$AgSb(S_xSe_{1-x})_2$	(220)	Ref.[29]
	51.5517	0.4434	1.7714	19.9	1.7688	Ag_5SbS_4	(351)	96-900-7511
	52.7340	0.2956	1.7344	30.0	1.7445	$AgSb(S_xSe_{1-x})_2$	(311)	Ref.[29]
	55.3202	0.3695	1.6593	24.3	1.6703	$AgSb(S_xSe_{1-x})_2$	(222)	Ref.[29]
	64.7783	0.3695	1.4380	25.5	1.4465	$AgSb(S_xSe_{1-x})_2$	(400)	Ref.[29]
	68.6207	0.3695	1.3666	26.0	1.3685	Ag_5SbS_4	(083)	96-900-7511
	71.5025	0.5911	1.3184	16.6	1.3122	Ag_5SbS_4	(600)	96-900-7511
	73.5714	0.3695	1.2864	26.8	1.2938	$AgSb(S_xSe_{1-x})_2$	(420)	Ref.[29]
	27.0197	0.3695	3.2973	22.1	3.3405	$AgSb(S_xSe_{1-x})_2$	(111)	Ref.[29]
	28.3498	0.2955	3.1456	27.7	3.1032	Ag_5SbS_4	(221)	96-900-7511
	31.3793	0.2217	2.8485	37.2	2.8930	$AgSbSe_2$	(200)	96-901-1029
	38.9163	0.5172	2.3124	16.3	2.2908	Ag_5SbS_4	(151)	96-900-7511
	39.9507	0.4433	2.2549	19.1	2.2576	Ag_5SbS_4	(133)	96-900-7511
	41.7980	0.4433	2.1594	19.2	2.1483	Ag_5SbS_4	(331)	96-900-7511
x=0.4	45.0493	0.2955	2.0108	29.1	2.0457	$AgSb(S_xSe_{1-x})_2$	(220)	Ref.[29]
	47.3399	0.2217	1.9187	39.1	1.9111	Ag_5SbS_4	(313)	96-900-7511
	51.2562	0.3694	1.7809	23.9	1.7688	Ag_5SbS_4	(351)	96-900-7511
	53.4729	0.3695	1.7122	24.1	1.7445	$AgSb(S_xSe_{1-x})_2$	(311)	Ref.[29]
	56.1330	0.5912	1.6372	15.2	1.6703	$AgSb(S_xSe_{1-x})_2$	(222)	Ref.[29]
	68.0296	0.5172	1.3770	18.5	1.3122	Ag_5SbS_4	(600)	96-900-7511
	73.7192	0.5912	1.2841	16.8	1.2938	$AgSb(S_xSe_{1-x})_2$	(420)	Ref.[29]
	26.9458	0.2956	3.3062	27.6	3.3405	$AgSb(S_xSe_{1-x})_2$	(111)	Ref.[29]
	28.4975	0.2955	3.1296	27.7	3.1032	Ag_5SbS_4	(221)	96-900-7511
	31.3054	0.2956	2.8550	27.9	2.8930	$AgSb(S_xSe_{1-x})_2$	(200)	Ref.[29]
	34.3350	0.8867	2.6097	9.4	2.6002	Ag_5SbS_4	(023)	96-900-7511
x=0.8	36.8473	0.5172	2.4373	16.2	2.4436	Ag_5SbS_4	(024)	96-900-7511
	38.9901	0.5172	2.3082	16.3	2.2908	Ag_5SbS_4	(151)	96-900-7511
	39.8030	0.4433	2.2629	19.1	2.2576	Ag_5SbS_4	(133)	96-900-7511
	41.7241	0.3694	2.1630	23.0	2.1483	Ag_5SbS_4	(331)	96-900-7511
	44.8276	0.2956	2.0202	29.1	2.0457	$AgSb(S_xSe_{1-x})_2$	(220)	Ref.[29]
	47.4877	0.2956	1.9131	29.4	1.9111	Ag_5SbS_4	(313)	96-900-7511

	48.3005	0.6651	1.8828	13.1	1.8840	Ag_5SbS_4	(204)	96-900-7511
	51.3300	0.6650	1.7785	13.3	1.7688	Ag_5SbS_4	(351)	96-900-7511
	53.1773	0.3694	1.7210	24.0	1.7445	$AgSb(S_xSe_{1-x})_2$	(311)	Ref.[29]
	55.6158	0.4433	1.6512	20.3	1.6703	$AgSbSe_2$	(222)	Ref.[29]
	61.1576	0.4433	1.5142	20.8	1.5036	Ag_5SbS_4	(045)	96-900-7511
	65.3695	0.6650	1.4264	14.2	1.4465	$AgSb(S_xSe_{1-x})_2$	(400)	Ref.[29]
	68.0296	0.5911	1.3770	16.2	1.3728	Ag_5SbS_4	(282)	96-900-7511
	72.0197	0.4434	1.3102	22.1	1.3122	Ag_5SbS_4	(600)	96-900-7511
	74.2365	0.5911	1.2765	16.9	1.2938	$AgSb(S_xSe_{1-x})_2$	(420)	Ref.[29]
	26.5764	0.2955	3.3513	27.6	3.3784	Ag_5SbS_4	(131)	96-900-7511
	28.5714	0.3695	3.1217	22.2	3.1032	Ag_5SbS_4	(221)	96-900-7511
	30.8621	0.3694	2.8950	22.3	2.9009	Ag_5SbS_4	(202)	96-900-7511
x=1.0	39.8768	0.5172	2.2589	16.3	2.2576	Ag_5SbS_4	(133)	96-900-7511
	44.2365	0.2955	2.0458	29.0	2.0423	Ag_5SbS_4	(114)	96-900-7511
	52.4384	0.2956	1.7435	30.0	1.7371	Ag_5SbS_4	(170)	96-900-7511
	54.8768	0.3694	1.6717	24.2	1.6812	Ag_5SbS_4	(063)	96-900-7511
	64.3350	0.2956	1.4469	31.7	1.4490	Ag_5SbS_4	(280)	96-900-7511
	73.0542	0.2956	1.2942	33.4	1.2926	Ag_5SbS_4	(283)	96-900-7511

Figs. 3 shows the X-ray diffraction patterns for $AgSb(S_xSe_{1-x})_2$ thin films for different sulfur content (x= 0.2, 0.4, 0.8, and 1.0), these patterns show that all films have amorphous structures, since all the patterns are absent from any diffraction peaks ,these results are in agreement with Wagner *et al*. [21], the amorphous structure related with low thickness of the prepared samples thin films , the structure may turn to poly crystalline with increase of thickness.

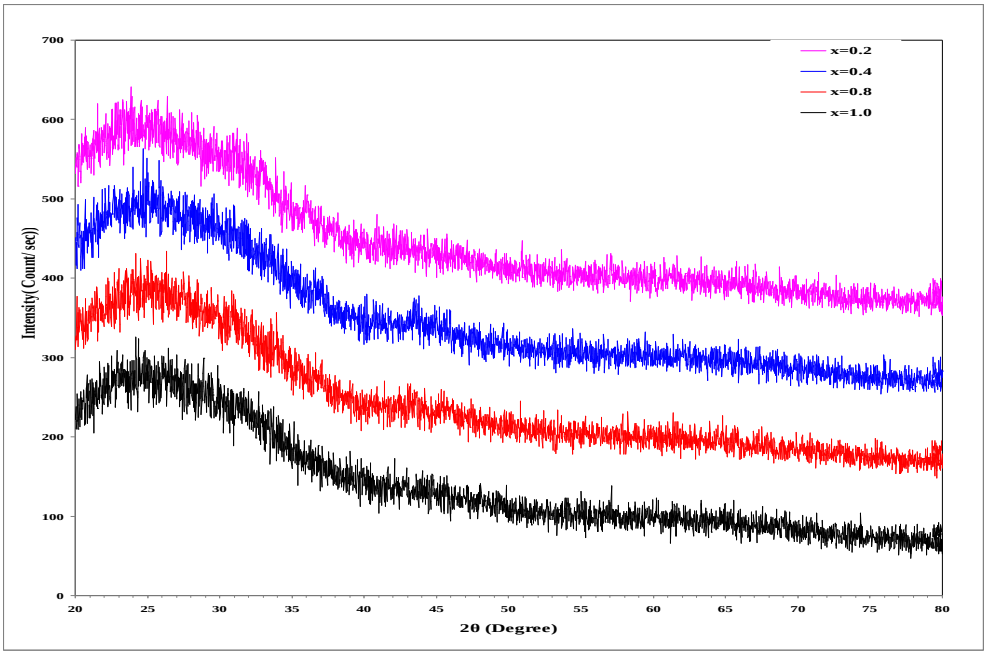

FIGURE 3: XRD of $AgSb(S_xSe_{1-x})_2$ thin films with different compositions

Atomic Force Microscopy Analysis (AFM)

The grain size (grain diameter) and average roughness of $AgSb(S_xSe_{1-x})_2$ thin films prepared by PLD with different sulfur content(0.2,0.4,0.8,and 1.0)have been measured using AFM as shown in Fig. 3. The measured grain size and RMS roughness are given in Table 3. This table shows the average grain size decreases with the increase of sulfur content, indeed average grain size decreases from 81.34 to 64.07 nm when sulfur content increases from 0.2 to 1.0. The roughness of the films shows non systematic change with the increase of sulfur concentration, moreover the values of surface roughness were found to increase from 0.857 to 0.951nm with increase of sulfur from 0.2 to 0.4 and then decrease to 0.675 nm with further increase of sulfur concentration.

TABLE 3: Average grain size and average roughness for $AgSb(S_xSe_{1-x})_2$ films with different thickness

x	Average roughness (nm)	Average grain size (nm)
0.2	0.857	81.34
0.4	0.951	79.09
0.8	0.250	75.40
1.0	0.675	64.07

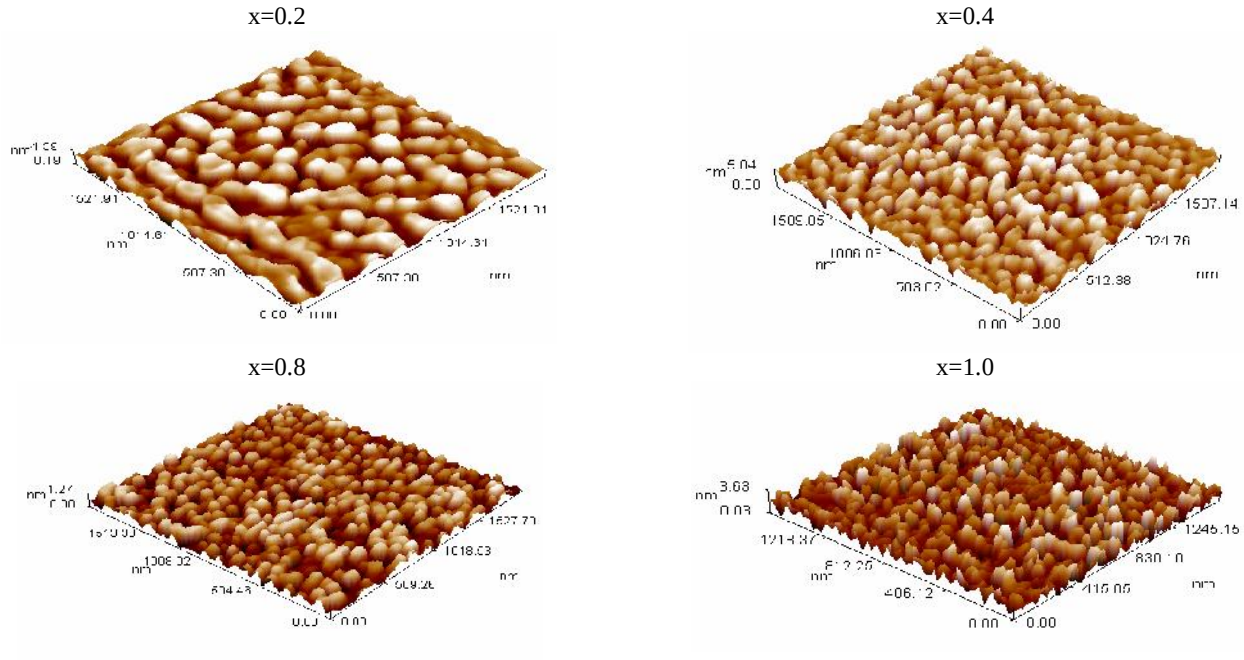

FIGURE 4: AFM pictures for $AgSb(S_xSe_{1-x})_2$ films with various sulfur content

The Optical Properties of $AgSb(S_xSe_{1-x})_2$ Films

The optical properties of the $AgSb(S_xSe_{1-x})_2$ thin films on glass for at room temperature with different sulfur concentration (0.2,0.4,0.8 and 1.0) nm have been determined using UV-visible near infrared transmittance spectrum in the region (300–1100) nm .The absorbance, transmittance and reflectance spectrum have been measured. The energy gap has been estimated.

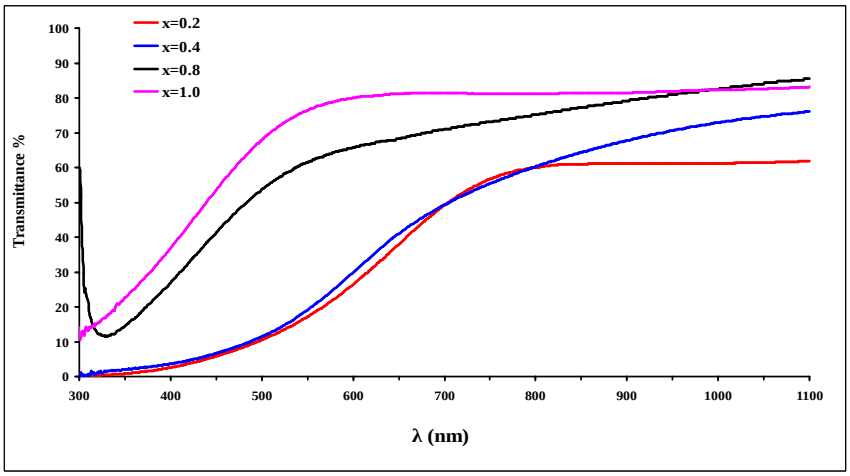

FIGURE 4: Transmittance versus wavelength of $AgSb(S_xSe_{1-x})_2$ thin films with various sulfur content

In general, we can observe from Fig. 4 that transmittance increases with increasing of sulfur concentration which means a decrease in the reflection and absorption also means that addition of sulfur make thin films sample more transparent and less absorbance. The shifts of transmittance toward shorter wavelength (higher energies) accompanied the increment of sulfur content is related with reduction of grain size, the reduction of grain size increases the lattice parameters and hence wide the energy gap as we seen in the next section.

The optical energy gap values E_g^{opt} for $AgSb(S_xSe_{1-x})_2$ thin films have been determined by using Tauc equation which is used to find the type of the optical transition by plotting the relations of $(\alpha hv)^{1/2}$, $(\alpha hv)^{1/3}$, $(\alpha hv)^{2/3}$ and $(\alpha hv)^2$ versus photon energy (hv) and selecting the optimum linear part. It is found that the relation for r =2 for allowed indirect transition yields linear dependence. The extrapolation *i.e.* E_g^{opt}, of the portion at $[(\alpha hv)^{1/2} = 0]$ is shown in Fig. 5. The value of the optical energy gap showed an increase of sulfur concentration, moreover E_g^{opt} increases from 1.10eV to 1.70eV when sulfur concentration increases from 0.2 to 1.0. This can be explained as follows ,noteworthy E_g^{opt} value of sulfur element is wide than selenium element , thus the increase of sulfur concentration in the film samples on the expense of selenium concentration leads to an increase of optical energy gap.

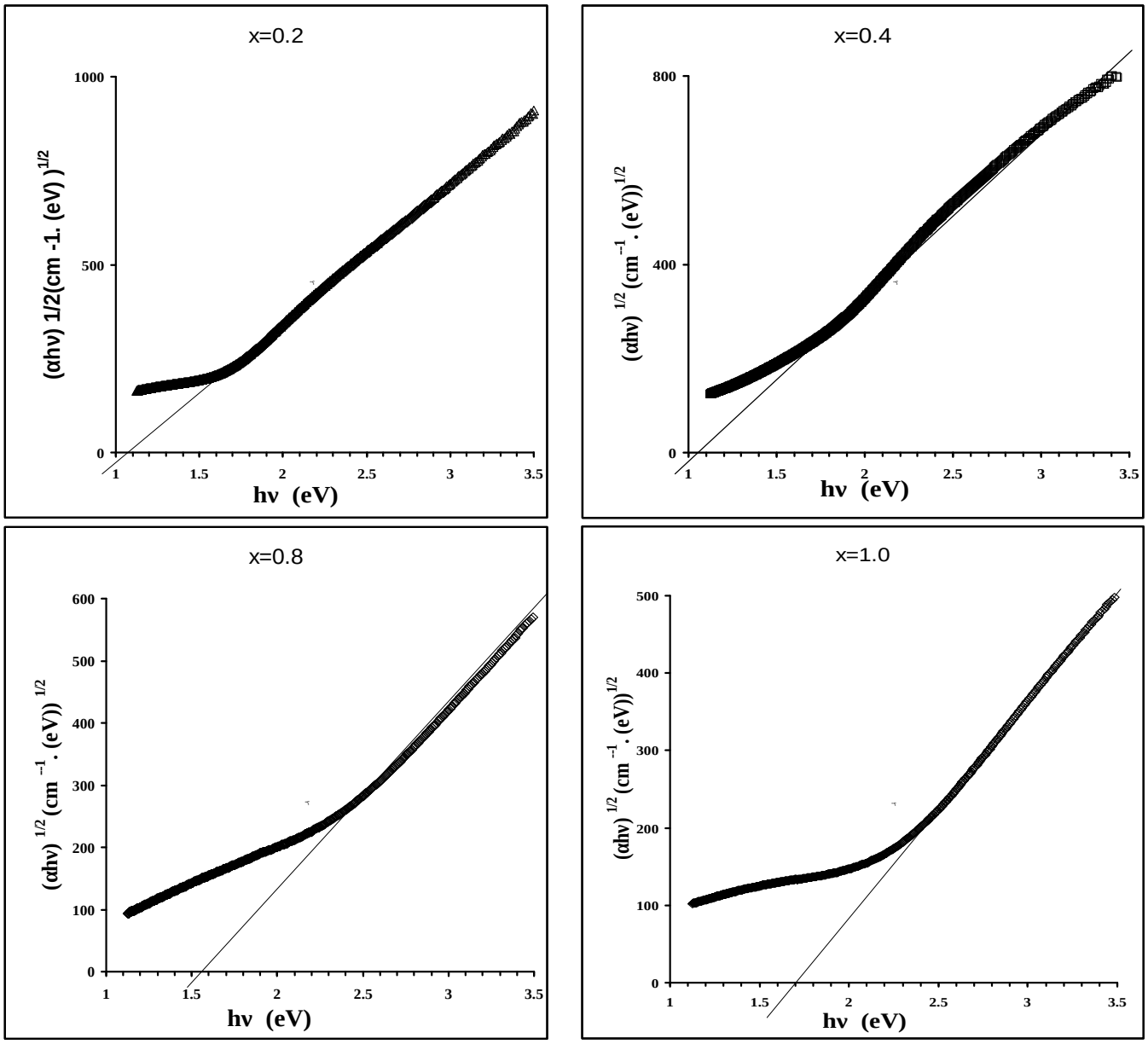

FIGURE 5: Relation between $(\alpha h\nu)^{1/2}$with (hν) of $AgSb(S_xSe_{1-x})_2$ thin films with various sulfur content

Dark and photoconductivity measurements of $AgSb(S_xSe_{1-x})_2$ *thin Films*

The current – voltage characteristics of the $AgSb(S_xSe_{1-x})_2$ thin films photodetectors with different sulfur content were measured at fixed intensity and plotted in Fig. 6 . The figures showed the photo current exceeded dark for law sulfur content photodetectors *i.e.* x=0.2, while poor photocurrent observed for sulfur content i.e. x=0.4. Photo conductivity takes apart when the incident light decreases the resistance of the sample throughout created new charge carriers. Thus, the increase of photo current is related to creation of new carries and henc reduction of potential barrier, which in turn increases mobility. In general the dark current increases with increasing voltage bias, but the increase at low voltage range was small due to the capturing, while increasing at high voltage range of the dark current increase with linear voltage where the defect states become in effective. The dark conductivity is σ_d and photo conductivity is σ_{ph} for $AgSb(S_xSe_{1-x})_2$ with two sulfur content (shown in table 4). The dark conductivity of the films increases two orders of magnitude with the increase of sulfur content. It is evident that $\Delta\sigma/\sigma$ for $AgSb(S_xSe_{1-x})_2$ sample for x=0.2 is higher than that at x=0.4 , this can be explained as follows: the localized states in the band gap considered as sensitive centers to the incident light as is responsible about photoconductivity, the increase of sulfur content in $AgSb(S_xSe_{1-x})_2$ thin films resulted in the compensate of these states , *i.e*. reduced the photoconductivity and hence to visual increase in the band gap.

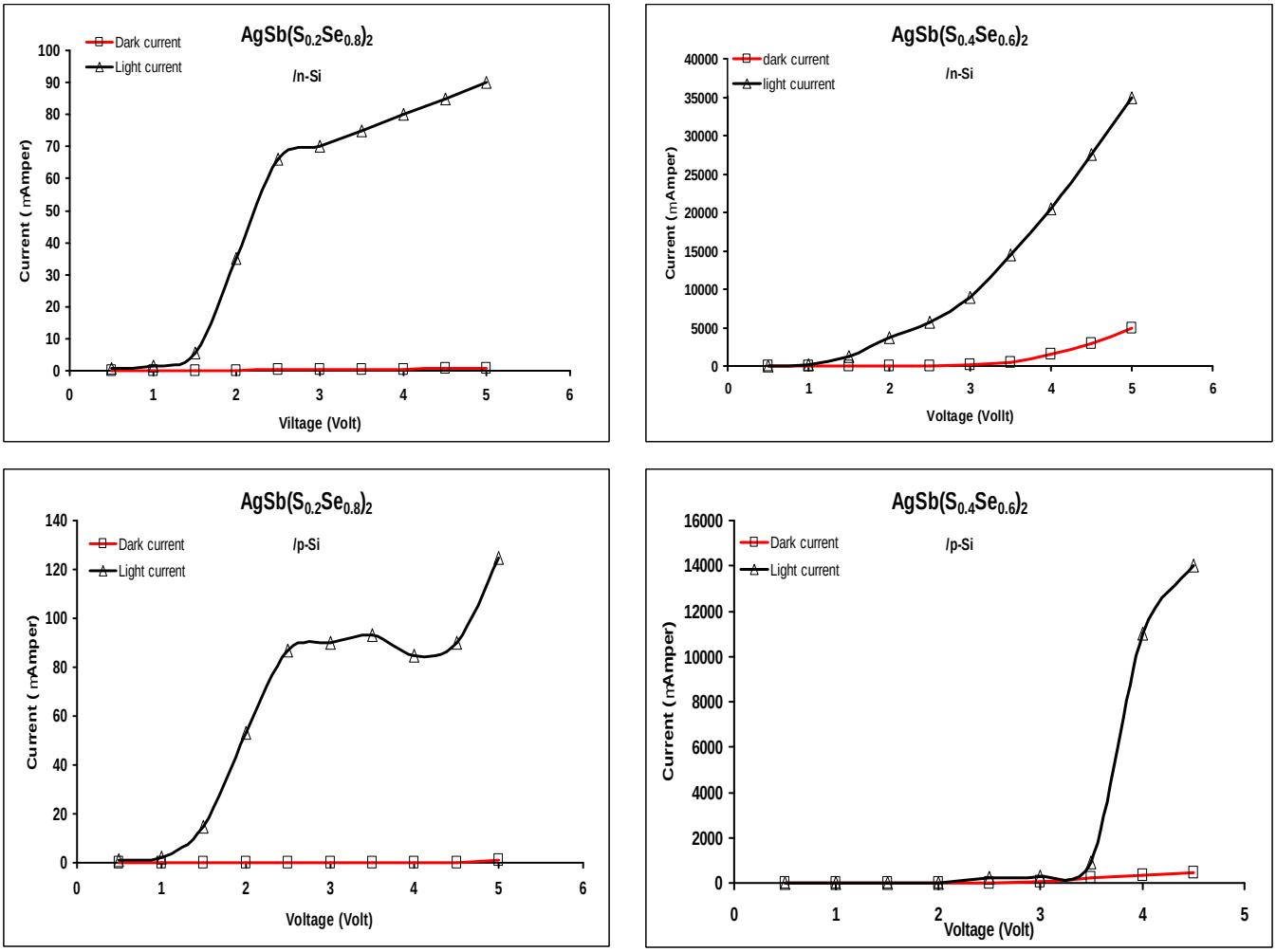

FIGURE 6: Variation of dark and photocurrent versus the applied voltage for $AgSb(S_xSe_{1-x})_2$ /n ,p-Si PC with various sulfur content.

TABLE 4: Dark-conductivity and photoconductivity of $AgSb(S_xSe_{1-x})_2$ thin films with various sulfur content

Photodtector sample	R_D (ohm)	R_L(ohm)	$\sigma_d(\Omega\cdot cm)^{-1}$	$\sigma_{ph}(\Omega\cdot cm)^{-1}$	$\Delta\sigma/\sigma$
$(AgSb(S_{0.2}Se_{0.8})_2$/n-Si	5.84E+06	4.38E+04	2.11E-09	2.82E-07	132.5
$AgSb(S_{0.4}Se_{0.6})_2$/n-Si	1.10E+03	1.29E+02	1.13E-05	9.55E-05	7.5
$(AgSb(S_{0.2}Se_{0.8})_2$ /p-Si	8.46E+06	3.74E+04	1.46E-09	3.30E-07	225.2
$AgSb(S_{0.4}Se_{0.6})_2$/ p-Si	8.74E+03	3.29E+02	1.41E-06	3.75E-05	25.5

I-V Measurements of $AgSb(S_xSe_{1-x})_2$ /n,p-Si heterojunction Figure .7 displays the behavior of current with reverse and forward for $(AgSb(S_{0.2}Se_{0.8})_2$/n-Si , $AgSb(S_{0.4}Se_{0.6})_2$/n-Si , $(AgSb(S_{0.2}Se_{0.8})_2$ /p-Si and $AgSb(S_{0.4}Se_{0.6})_2$/ p-Si heterero junctions. The forward current is related to the flow of majority carriers which resulted in reduction of the built - in potential, as well as the width of the depletion layer, this region consisted of two regions, the law voltage range(0-0.1) Volt ,where the recombination current is dominated , and the high voltage region (>0.1Volt) where tunneling current is dominated. Also the reverse current is consisted of two regions, the law voltage region (<0.1 Volt), the generation current dominates and the high voltage region (>0.1 Volt), the diffusion current is dominating. It is obvious that dark current of $(AgSb(S_{0.2}Se_{0.8})_2$ and $(AgSb(S_{0.4}Se_{0.6})_2$ cells deposited on n-Si substrates exceeded that of residual samples ,this may ascribed to the good matching between the window and absorber layers . The ideality factor (β) measured from the slope in law voltage region using the equation $= \frac{q}{slope(\ln I_d / V) * k_B * T}$, the values of ideality factor gives indication about the defects in the junction. The ideality factor shown in Figure.8 that gives indication that $AgSb(S_{0.4}Se_{0.6})_2$ /p-Si which exhibits lower β is promise cell for photovoltaic application . The variation of current with applied voltage when $AgSb(S_xSe_{1-x})_2$ /n,p-Si cells illuminated with white light is shown in Figure. 9. The measurements were done out under illumination with power intensity equal to (105) mW/cm^2. From this figure it is clear that the photocurrent increases with increasing of the bias voltage. This can be due to high level injection of carriers such that the applied voltage is no longer totally developed across the depletion region. At the high reverse biasing break down can occur due to impact ionization or zener tunneling.

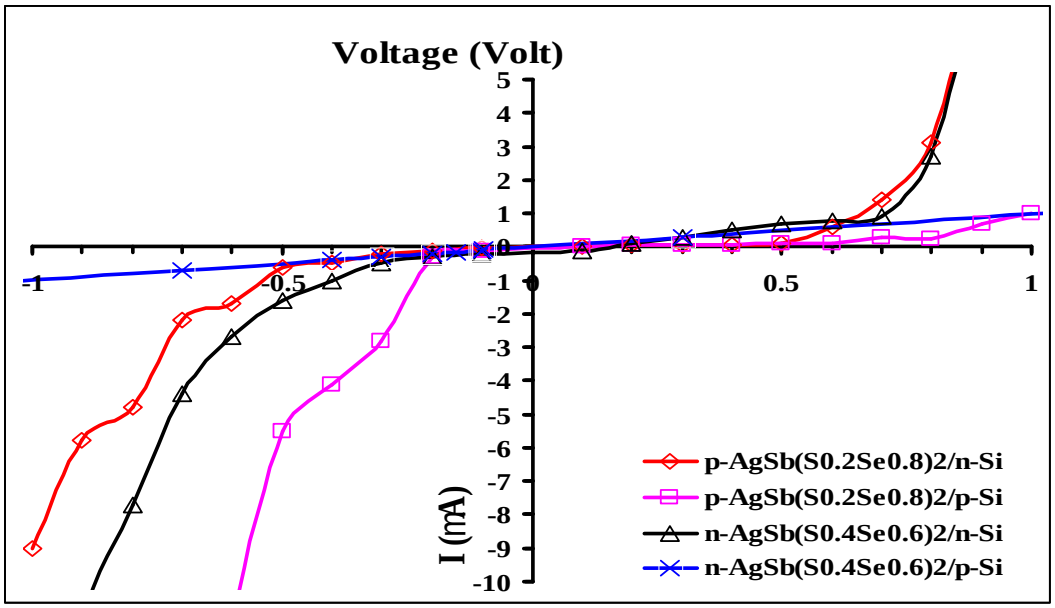

FIGURE 7: I-V characteristics in dark for $AgSb(S_xSe_{1-x})_2$ /n, p-Si heterojunction with different sulfur content.

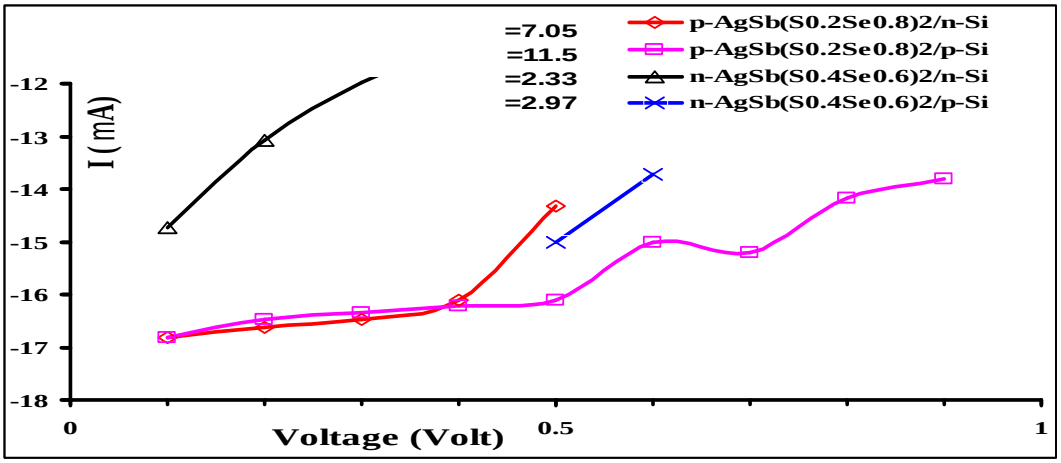

FIGURE 8: Relation beween Ln(I) and the bias voltage for $AgSb(S_xSe_{1-x})_2$ /n,p-Si heterojunction with different sulfur content.

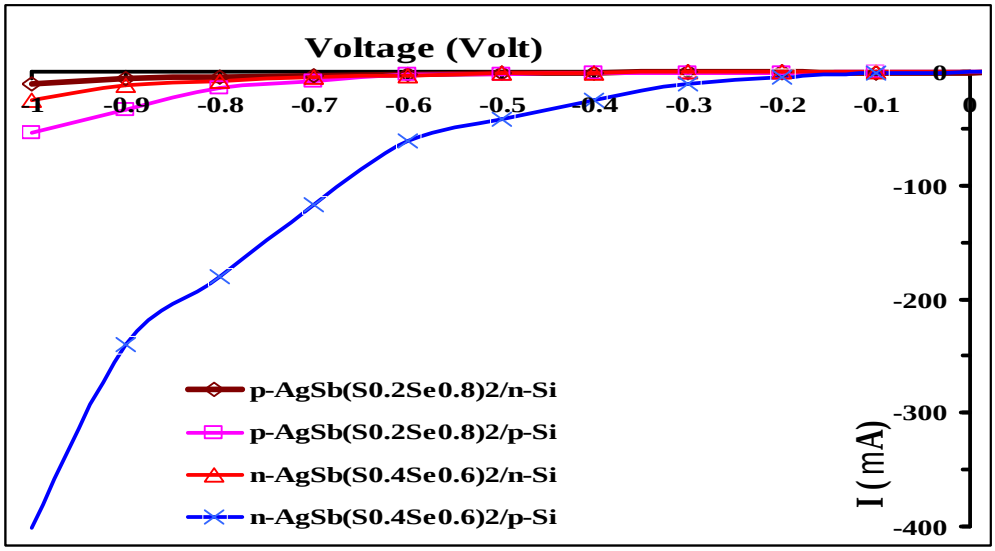

FIGURE 9: Figure.9 The current – Voltage characteristics for $AgSb(S_xSe_{1-x})_2$ /n,p-Si heterojunction under illumination with different sulfur content.

CONCLUSION

The present study deduces the following:

1. It was successfully obtained the quaternary alloys as seen from X-ray diffraction.
2. Amorphous thin films of $AgSb(S_xSe_{1-x})_2$ was provided from PLD.
3. Grain size was reduced by the increasing of sulfur content $AgSb(S_xSe_{1-x})_2$ thin films which result in proceeding increase of the band gap of indirect allowed transition.
4. Thin films of $AgSb(S_xSe_{1-x})_2$systems become more transparent to the incident light by the increasing of sulfur concentration.
5. $AgSb(S_{0.2}Se_{0.8})_2$/n,p-Si thin films showed optimum performance as photodetector .

REFERENCES

[1]. B. Yang, L. Wang, J. Han, Y. Zhou, H. Song, S. Chen, J.Zhong, L. Lv, D. Niu, and J. Tang, Chem. Mater. **26**(10), 3135-3143 (2014).

[2]. J.G. Garza, S. Shaji, A.C. Rodriguez, T.K. Das Roy, and B.Krishnan, Appl. Surf. Sci. **257**(24), 10834-10838 (2011).

[3]. J.O. González, S. Shaji, D. Avellaneda, G.A. Castillo, T.K.Das Roy, and B. Krishnan, Appl. Phys. A **116**(4), 2095-2105 (2014).

[4]. K. Bindu, M.T.S. Nair, T.K. Das Roy, and P.K. Nair, Electrochem. Solid-State Lett. **9**(6), G195-G199 (2006).

[5]. J.O. González, S. Shaji, D. Avellaneda, A.G. Castillo, T.K. Das Roy, and B. Krishnan, Mater. Res. Bull. **48**(5), 1939-1945 (2013).

[6]. E. Dassau, B. Grosman, and D.R. Lewin, Comp. Chem. Eng. **30**(4), 686-697 (2006).

[7]. A.G. Gevorkyan, G.E. Shter, and G.S. Grader, Thermochim. Acta **605**, 107-114 (2015).

[8]. I. Klugius, R. Miller, A. Quintilla, T.M. Friedlmeier, D. Blázquez-Sánchez, E. Ahlswede and M. Powalla, Thin Solid Films **535**, 107-111 (2013).

[9]. J. Koo, S. Jeon, M. Oh, H.-I. Cho, C. Son, and W.K. Kim,Thin Solid Films **535**, 148-153 (2013).

[10]. S.C. Kim, J. Koo, and W.K. Kim, Thin Solid Films **531**, 233-237 (2013).

[11]. H. Simchi, B.E. McCandless, K. Kim, and J.H. Boyle, Thin Solid Films **535**, 102-106 (2013).

[12]. M.G. Sousa, A.F. da Cunha, P.A. Fernandes, J.P. Teixeira, R.A. Sousa, and J.P. Leitão, Sol. Energy Mater. Sol. Cells**126**, 101-106 (2014).

[13]. T.K. Bera, J.-H. Song, A.J. Freeman, J.I. Jang, J.B. Ketterson, M.G. Kanatzidis, Angew. Chem. Int. Ed. 47 (2008) 7828e7832.

[14]. T.K. Bera, J.I. Jang, J.-H. Song, C.D. Malliakas, A.J. Freeman, J.B. Ketterson, M.G. Kanatzidis, J. Am. Chem. Soc. 132 (2010) 3484e3495.

[15]. M. Hamam, Y.A. El-Gendy, M.S. Selima, N.H. Teleba, A.M. Salema, Chalcogenide Lett. 6 (2009) 359e365.

[16]. J. Gutwirth, T. Wagner, P. Nemec, S.O. Kasap, M. Frumar, J. Non Cryst. Solids, 354 (2008) 497e502.

[17]. A.M. Ibrahim, J. Phys. Condens. Matter 7 (1995) 5931e5938.

[18]. T. Wagner, J. Gutwirth, P. Nemec, M. Frumar, T. Wagner, M. Vlcek, V. Perina, A. Mackova, V. Hnatovitz, Appl. Phys. A 79 (2004) 1561e1562.

[19]. E.R. Baranovaa, V.L. Kobelev, O.L. Kobeleva, L.L. Nugaeva, V.B. Zlokazov, L.Ya. Kobelev, Solid State Ionics 146 (2002) 415e421.

[20]. I. Kelleher, S.A. Redfern, R.A.D. Pattrick, Mineral. Mag. 60 (1996) 393e401.

[21]. H. Effenberger, W.H. Paar, D. Topa, A.J. Criddle, M. Fleck, Am. Mineral. 87 (2002) 753e764.

[22]. A. Orliukas, V. Valiukenas, V. Kybartas, A. Kezionis, Ferroelectrics 38 (1981) 897e900.

[23]. P.J.S. Ewen, in: Photo-induced meta stabilty in Amorphous (ed. A.V. Kolobov), Wiley-VCH, Weinheim, p. 365.

[24]. T. Kawaguchi, in Photo-induced metastabilty in Amorphous (ed. A.V. Kolobov), Wiley-VCH, Weinheim, p. 182.

[25]. T. Wagner, J. Gutwirth, T. Kohoutek, M. Krbal, P. Bezdicka, J. Pokorny, M. Vlcek, M. Frumar, Optically-induced Photodarkening and Photocry-stalli-zation in Amorphous Ag-Sb-S Films Prepared by Three Deposition Techniques,

[26]. K Bindu, Jos´e Campos, M T S Nair, A S´anchez and P K Nair, Semiconducting $AgSbSe_2$ thin film and its application in a photovoltaic structure, Semicond. Sci. Technol. 20 (2005) 496–504.

[27]. J. Tasseva, V. Lozanova, R. Todorov, K. Petkov' Journal of Optoelectronics and Advanced Materials, Optical characterization of Ag/As-S-Se thin films Vol. 9, No. 10, October 2007, p. 3119 – 3124.

[28]. Bushra A. Hasan, Investigation the Structural and Optical Properties of $AgSbSe_2$ Photoconductor, Australian Journal of Basic and Applied Sciences, 9(23) July 2015, Pages: 97-104.

[29]. Dorian Leonardo Rodriguez Vela, Bindu Krishnan, Josue Amilcar Aguilar Martinez, Shadai Lugo Loredo, and Sadasivan Shaji, $AgSb(S_xSe_{1-x})_2$ thin films by rapid thermal processing of Sb_2S_3-Ag-Se thin films for photovoltaic applications, hys. Status Solidi C **13**, No. 1, 47–52 (2016)/ **DOI** 10.1002/pssc. 201510117.